JES Focus Issue on Ubiquitous Sensors and Systems for IoT

Low Cost Inkjet Fabrication of Glucose Electrochemical Sensors Based on Copper Oxide

R. Bernasconi,* A. Mangogna, and L. Magagnin **,z

Dipartimento di Chimica, Materiali e Ingegneria Chimica Giulio Natta, Politecnico di Milano, 20131 Milan, Italy

The availability of low cost, efficient and wearable glucose sensors is one of the prerequisites for the development of ubiquitous sensors networks for the efficient monitoring of diabetes epidemiology. Starting from this principle, wet metallization and low cost inkjet printing were employed in the present work to manufacture non-enzymatic electrochemical sensors. CuO nanoparticles were inkjet printed on platinum, which was electrodeposited on stainless steel. The active layer obtained in this way showed an acceptable linear range for glucose detection and a good sensitivity when used as sensor. The influence on performances of interfering species and curvature were investigated, demonstrating a negligible effect for the first and a decrease in linearity of the response and sensitivity for the latter.

 [DOI: 10.1149/2.0241808jes]

Manuscript submitted February 12, 2018; revised manuscript received April 16, 2018. Published May 17, 2018. *This paper is part of the JES Focus Issue on Ubiquitous Sensors and Systems for IoT.*

In a world where population grows and lifespan continuously increases,[1] providing efficient healthcare to everybody is one of the main challenges. One of the possible strategies to manage the increasing number of patients is to limit hospital admissions to the medical cases where the physical presence of the patient is unavoidable, like in the case of surgery. Many other tasks, like diagnostic services or post operation monitoring that are nowadays performed requiring the patient to reach a clinic, can be easily performed at home with no risk for the health.[2] Home health monitoring (HHM)[3] presents three main advantages: the patient does not move from home, medical facilities occupation and personnel usage are reduced and continuous monitoring can be performed. The HHM approach is currently widely used and many kinds of portable medical devices,[4,5] like compact sphygmomanometers[6] or portable glucose sensors,[7] allow the home control of patients.

The next step in the delocalization of home monitoring may be the introduction of some technologies of the developing Internet of Things (IoT),[8] like ubiquitous sensors networks (USNs).[9] If the medical instruments used by the patients to monitor their health status are made IP addressable[10,11] and is provided the ability to transmit data in a unified network via the internet, they can be used to build a real time healthcare network, which can in principle be global.[12,13] By doing this, the impact and evolution of diseases could be monitored on a large scale, allowing thus the selection of proper therapeutic strategies.[14–17] Moreover, wireless connected medical sensors could trigger a real time intervention for the single patients in case of emergency (thanks to their connection with medical facilities).[18–21] Finally, application of sensors to people that are at risk for a specific disease, e.g. cardiovascular pathologies,[22,23] may increase prevention and allow the statistical evaluation of the disease incidence on the population. The creation of USNs monitoring individual human health in daily life is therefore an interesting topic for current research.

An interesting application in healthcare for USNs is ubiquitous glucose sensing in blood for diabetes[24] treatment. It was estimated that the world population affected by diabetes, both I and II type, is around 415 million,[25] with an increasing trend observed in the last few years. Since diabetic patients constitute a significant percentage of the population, it is advantageous to provide a USN to monitor their conditions in real time and to evaluate the global epidemiology of the disease.[26–28] A smart sensors network could be used to optimize insulin administration, possibly under remote control by a doctor, or to provide emergency hospitalization in case of emergency.[29,30] Glucose sensors may also be combined with other sensors to provide a more complete monitoring coverage.

To allow the creation of a real USN, certain characteristics are required to the glucose sensors employed. First, they should be wearable to allow the possibility of continuous monitoring minimizing the discomfort for the patient. This means that the devices must be at least flexible, preferentially also stretchable, to adapt to the body. Another important requirement for the sensors is the low cost. To make possible a widespread diffusion, cost of the single device must be kept very low. In addition, production route followed to manufacture the sensor should allow a certain degree of customizability. Finally, the working principle and the structure of the sensor should be as simple as possible. These requirements suggest the class of electrochemical non-enzymatic sensors[31,32] as ideal candidates for USNs glucose sensing. Many detection methods exist,[33–35] but electrochemical devices are characterized by a series of attractive properties: low cost, high sensitivity, long shelf life and simple architecture. Moreover, the absence of enzymes avoids problems of immobilization instability and reproducibility over time. Typically, a metal, both precious and non-precious, constitutes the material on which the glucose oxidation reaction exploited for sensing takes place.[32,36] Recently, however, the possibility to use metal oxides,[36,37] graphene[38,39] and other materials was demonstrated. Copper oxide constitutes an example of these alternative materials, being a p-type semiconductor with comparatively narrow bandgap (1.2 eV). CuO is a good material for glucose sensing due to its high catalytic activity toward glucose oxidation and due to its low cost.[34] Many reports are available on devices that employ CuO nanoparticles (NPs),[40–43] nanospheres[44] or other forms of this metal oxide.

The main aim of the present work is the realization of CuO NPs based sensors analogous to existing state-of-the-art devices,[40,43] characterized by flexibility and considerably reduced low cost, in accordance to the requirements of USN glucose sensing. A single use approach is followed: the active part of the device is intended to be disposed after a certain period of use, while readout circuitry can be reused. Single use sensors present many advantages in terms of hygiene and performance stability with time. To keep the cost of the sensor as low as possible, wet metallization techniques and inkjet deposition from household printers were employed. Such low cost approach is also ideal to allow product customizability according to the specific needs of the patient. Final goal is to replicate the same performances of sensors fabricated with more elaborated techniques.[40,43] Initially, inkjet printability of CuO nanoparticles was analyzed and the morphology of printed CuO layers was investigated. Inkjet printing

*Electrochemical Society Student Member.
**Electrochemical Society Member.
zE-mail: luca.magagnin@polimi.it

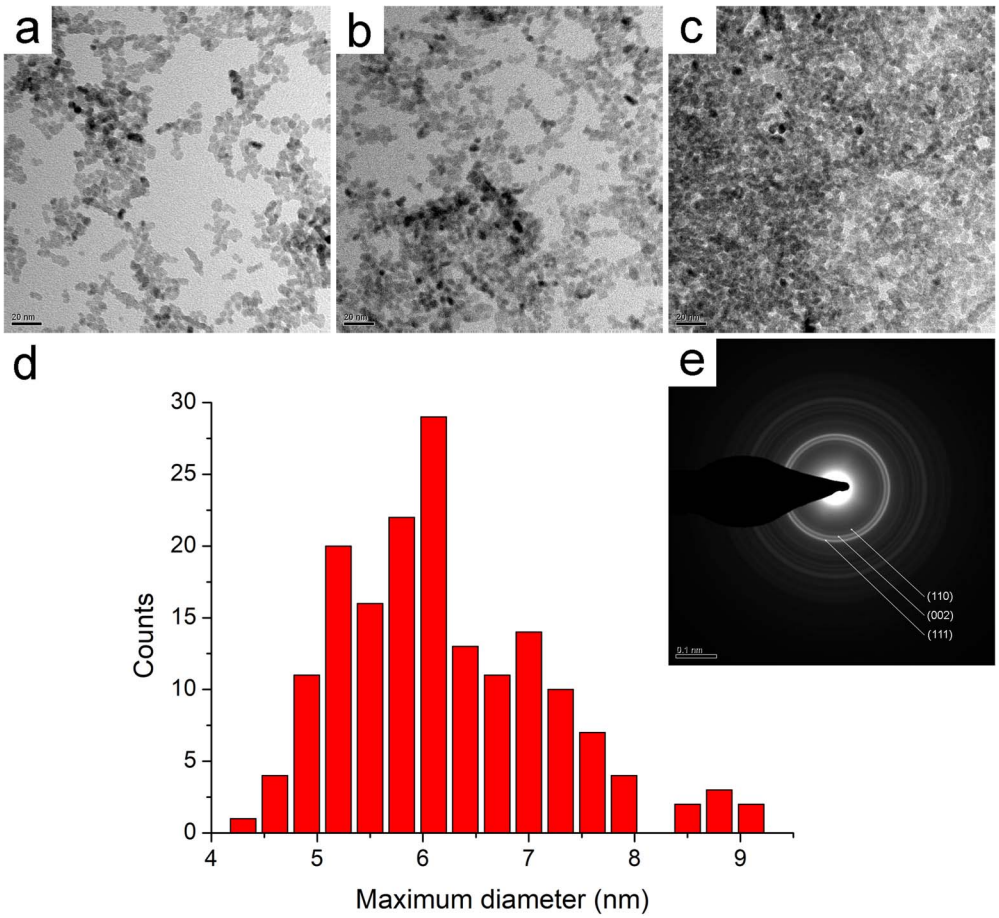

Figure 1. TEM images of aggregates formed in inks containing 1% wt CuO NPs and 5% wt (a), 10% wt (b) and 20% wt (c) EG; size distribution of the major diameter of CuO NPs (d); SAED pattern of CuO NPs (e).

was then transferred to the production of thin film glucose sensors. Embedded counter and reference electrodes were not realized, concentrating all the attention on the inkjet printed active material and its properties. Microstructure and functionality of these sensors were investigated to determine their sensitivity and detection limits.

Experimental

All the chemicals employed in the work were purchased from Sigma Aldrich and used as received. The 25 μm thick AISI 302 stainless steel (SS) sheet was acquired from Precision Brand. CuO NPs were synthesized in water phase.[40,45] As first step of the synthesis route, 1 ml of pure CH_3COOH was added to 200 ml of 0.2 M $Cu(CH_3COO)_2$. Resulting solution was heated to 100°C and 1 g of NaOH was added under vigorous stirring. Solution changed its color from blue to black and it was cooled to room temperature. The black precipitate obtained was centrifuged (4000 rpm; 1 minute), washed with deionized water and ethanol and dried on a heater. CuO NPs inks were formulated containing different amounts of CuO (0.5% wt, 1% wt or 2% wt) or ethylene glycol (EG) (5% vol., 10% vol. and 20% vol.). Ink preparation was performed mixing first water and EG in the desired volumetric concentration and then adding CuO. Weight percentage of CuO NPs is therefore referred to the final weight of water/EG + CuO mixture. The ink was then stirred for 24h and finally sonicated for 30min using a Falc Instruments sonicator (50 kHz; 100 W). A commercial PixmaMX495 printer by Canon was employed for inkjet printing of CuO NPs. Commercial cartridges were filled with CuO NPs ink and then sealed to avoid leaks. The ink was printed with a maximum resolution of 4800 × 1200 dpi (dots per inches) and a monochromatic printing speed of 9.9 ipm (images per minute). Pt/Ni coated SS substrates were fixed with adhesive tape on paper sheets to perform inkjet printing. Before inkjet printing, Ni was deposited on SS using a Wood strike bath composed of 250 g/l nickel chloride hexahydrate and 250 ml/l hydrochloric acid (32% wt commercial solution). Before plating, surface was dipped in a 20% vol. hydrochloric acid solution for 30 seconds. Ni deposition was performed at room temperature, at 400 mA/cm^2 and for 1 minute. A strong stirring was employed to efficiently remove the gas forming on the surface. Pt was deposited on Ni employing a bath containing 0.02 M chloroplatinic acid hexahydrate, 0.5 M trimethylamine, 0.5M potassium nitrate and 0.2 M dipotassium monohydrogen phosphate. Deposition was performed at pH 11.5, 60°C, 20 mA/cm^2 for 10 minutes. Plating of both Pt and Ni was performed using mixed oxides coated Ti nets as anodes. Inkjet printing of CuO NPs was performed on the final Pt layer. Printed samples were subjected to an annealing at 150°C for 30 min.[40] To use it as a sensor, the SS substrate with the different layers on top was glued to a 100 μm thick PET sheet. Subsequently, a Kapton adhesive sheet presenting a 5 mm/5 mm window was applied to the sensor to determine the active area. Cyclic voltammetry (CV) and chronoamperometry (CA) measurements were performed using an EG&G potentiostat/galvanostat by Princeton Applied Research. Electrochemical measurements were at room temperature in 0.1 M sodium hydroxide solution with a Pt counter electrode and an Ag/AgCl saturated electrode as reference. CV measurements were carried out on the CuO covered electrode in absence and presence of glucose at scan speed of 50 mV/s. CA measurements were carried at + 0.5 V with 1 mM glucose additions every 45 s with stirring. CA measurements were also performed on two curved surfaces with different radius of curvature, 15 mm and 30 mm respectively. The calibration curve was established using the data obtained from CA measurements

performed adapting the surface of the sensor to the curvature and fixing the shape obtained with adhesive tape. In the case of interference tests, some selected sugars were added to the 0.1 M sodium hydroxide solution together with glucose. Lactose, mannitol, maltose, sorbitol and fructose were employed. Two tests with two distinct concentrations of such interfering sugars, 0.01 mM and 0.02 mM, were employed; 0.5 mM was selected as glucose concentration. Contact angle was evaluated employing a camera to acquire images of droplets dispensed from a needle. The Drop Shape analysis software was used to evaluate contact angle. Rheological characterization was performed using a Rheometrics DSR200 (Dynamic Stress Rheometer) with planar plates. A shear rate of 400 s^{-1} was applied, acquiring the mean dynamic viscosity value. A EVO 50 EP by Zeiss SEM, coupled with a Inca Energy EDS unit was used to investigate the morphology and composition of the layers. TEM was performed employing a Philips CM 200. The instrument used to acquire AFM topographical data was a NT-MDT SOLVER PRO.

Results and Discussion

CuO nanoparticles characterization.—CuO nanoparticles from synthesis were used to make up inkjet inks. For this reason, their morphology, size distribution and aggregation behavior were evaluated. Figure 1a shows the morphology of the nanoparticles observed using TEM. 1% wt CuO NPs were dispersed in a water/ethylene glycol mixture at different concentration, namely 5% wt (Figure 1a), 10% wt (Figure 1b) and 20% wt (Figure 1c) EG. Glycols are typically added to inks for jetting as humectants and rheology modifiers.[46] For this reason, EG was selected in the formulation of the ink used in the present work to increase viscosity and to avoid premature nozzle clogging. All the inks formulated were found to be stable for days, with no CuO NPs precipitation observed. From the morphological point of view, CuO particles were characterized by an almost equiaxial shape. Size distribution of the major diameter of the particles, reported in Figure 1d, was characterized by a mean value around 6 nm. CuO nanoparticles were found to be polycrystalline and phase pure according to their SAED pattern (Figure 1e), which evidenced the presence of only monoclinic CuO.[47] Diffraction rings for CuO (110), (002) and (111) planes are clearly visible in Figure 1e. Different aggregation behaviors were evidenced by analyzing TEM images obtained evaporating the three different inks at increasing EG content. Tendency to agglomerate was greatly amplified by a high EG content, as visible from Figures 1a, 1b and 1c. Apparently, NPs concentration looks different observing the three images. However, the effect is solely due to different behavior of the mixture when it evaporates, leaving the CuO nanoparticles in different aggregation states.

Ink printability.—Initially, ink printability was evaluated by simply increasing CuO concentration: 0.5% wt, 1% wt and 2% wt concentrations were employed. Since a commercial office inkjet printer was used, printing quality was evaluated visually using paper sheets first and then the SS/Ni/Pt substrates. In general, the inks obtained at the different concentrations were always printable on paper, but final quality varied. At 0.5 and 1% wt the quality of the coating was good and the printing was uniform. Conversely, at 2% wt, printing was less uniform and horizontal stripes started to appear on the printed surface. Such imperfections were typically observed when the flux of the ink in some nozzles was irregular. As a consequence, they jetted the fluid in an irregular way, leaving stripes on the printed surface. In addition, reproducibility decreased at 2% wt CuO, with some samples more uniform than others. The phenomenon described took place at all EG concentrations. To avoid this effect and to maximize CuO concentration in the ink, 1% wt was therefore selected as optimal concentration. No major effects on final quality were observed when the CuO ink was printed on paper. Conversely, printing on Pt was found to be optimal at low EG concentrations. An ink containing 20% wt EG was found to yield less uniform layers due to partial droplets coalescence on the surface. Final result was the appearance of areas with higher thickness close to areas with almost no ink. This phenomenon can be easily explained

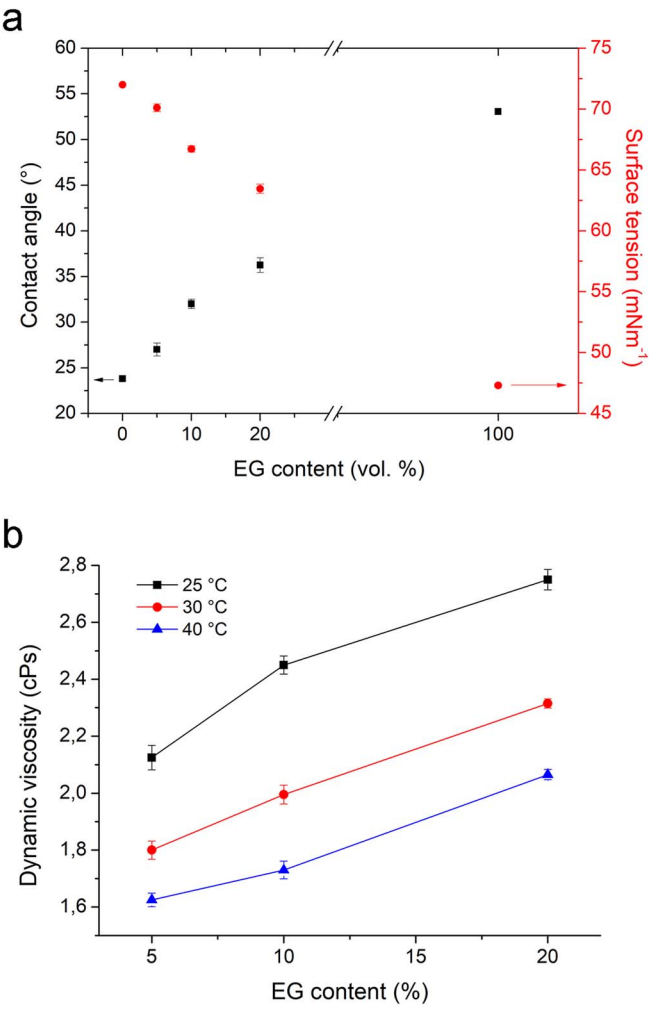

Figure 2. Contact angles measured on gold and surface tension of the three CuO inks as a function of EG content (a; water and EG values from literature are reported for comparison); Dynamic viscosity of the three CuO inks as a function of EG content (b).

considering the contact angle values on Au reported in Figure 2a. By increasing EG content, contact angle increases too, reducing thus surface tension. However, Pt is highly wettable, having a contact angle around 5° (with water). High EG inks droplets tend therefore to coalesce on the surface due to the low wettability. A 10% wt EG concentration, which optimizes printing quality and viscosity, was selected as optimal for printing. To characterize printability in a more quantitative way, the most significant ink parameters were determined and intercorrelated by calculating the Onhesorge number. The inverse of this number is widely used to evaluate printability of solutions.[48] Contact angles were measured on gold using water, EG and the three inks. Results obtained are reported in Figure 2a. Surface tension was extrapolated using the well-known Young relationship (Equation 1).

$$\gamma_s = \gamma_{sl} + \gamma_l \cos\theta \quad [1]$$

γ_s is the surface energy of the solid, γ_{sl} is the interfacial energy solid/liquid, γ_l is the surface tension of the liquid and θ is the contact angle. γ_s is constant, because the substrate is always gold. Therefore, Equation 1 can be transformed, for two different fluids a and b, in Equation 2.

$$\gamma_{sl,a} + \gamma_{l,a} \cos\theta_a = \gamma_{sl,b} + \gamma_{l,b} \cos\theta_b \quad [2]$$

Rigorously, $\gamma_{sl,a}$ and $\gamma_{sl,b}$ are unknown. If surface wetting for the two fluids is relatively low, however, γ_{sl} values are small and similar. In a first rough approximation, considering such similar order

Table I. Surface tension, density, dynamic viscosity and Ohnesorge number for three inks formulated. Values for water and EG are reported for comparison.

Fluid	Surface tension (mN m^{-1})	Density (Kg m^{-3})	Dynamic viscosity (cPs)	Z
H_2O	72.00	1000	0.89	30.15
5% EG wt + 1% CuO	70.11	1004	2.13	12.48
10% EG wt + 1% CuO	66.73	1015	2.45	10.62
20% EG wt + 1% CuO	63.45	1026	2.75	9.28
EG	47.30	1110	16.9	1.36

of magnitude, $\gamma_{sl,a}$ and $\gamma_{sl,b}$ can be neglected in Equation 2. If this process is carried out, unknown surface energy of a fluid can be calculated if surface energy of another fluid is known, along with the respective contact angles on gold. Results obtained are reported in Table I. Values obtained are almost identical to literature data for water/EG mixtures (without CuO) available from literature.[49] This is somewhat expected, because CuO NPs are relatively inert and in suspension in the ink in a low amount. It is therefore reasonable that they do not alter significantly surface tension with respect to corresponding pure water/EG solutions.

Dynamic viscosity was evaluated as well using a shear rheometer (Figure 2b). As expected, viscosity increases with EG content and decreases with temperature. EG has a viscosity higher than water, and for this reason water/EG mixtures present a viscosity that increases with EG concentration. Temperature dependence of viscosity is typically observed in most fluids.[50] A shear rate dependent behavior of the ink was observed as well. This non-linear effect may be due to the fact that the ink is a suspension of particles and not an homogeneous fluid.[51] Finally, the inverse of Ohnesorge number was evaluated according to Equation 3.

$$Z = \frac{1}{Oh} = \frac{\sqrt{a\rho\gamma}}{\eta} \quad [3]$$

ρ, γ, and η represent density, surface tension, and dynamic viscosity of the fluid respectively. a is the characteristic dimension, in this case the diameter of the nozzle, which was set at 10 μm. Table I recaps all the parameters for the different inks and for the two pure substances that constitute the base of the inks themselves. Fromm demonstrated that stable drop formation in inkjet systems is possible only for Z values higher than 2.[52] However, inks present optimal printability only for Z values higher than 4 and lower than 14.[48] It was observed in particular that fluids presenting Z values higher than 14 were unable to form single droplets and were invariably characterized by satellite drops. As expected, the use of water/EG mixtures brings ink printability in the suitable range, with all the inks formulated having Z values comprised between 4 and 14. Water and EG alone are printable too, but Z values too high or too low may lead either to unstable drop formation or to the presence of satellite drops.

Printed layers characterization.—CuO NPs were inkjet printed on Pt, electrodeposited on SS with the interposition of a Wood Ni strike layer. CuO thickness was tuned by changing the number of printing steps. Alignment problems may rise during multiple layers printing, since the paper handling system of the office printer employed is not designed to align sheets for sequential printing. It was found however that, by carefully loading paper in the printer tray and by maintaining clean the drums that move the paper, alignment tolerances between 100 and 150 μm can be easily achieved. Figure 3a depicts the SEM morphology of a CuO layer obtained with 25 printing steps. The uniformity of the CuO coating was in general good due to the already cited low contact angle of the as plated Pt surface, which is around 5° with water. Good wettability avoids droplets coagulation and yields a good coating quality. The formation of sub-micrometric aggregates on the surface of the coating was observed from SEM analysis (Figure 3a). Such structures may be either present in the ink before jetting, as a consequence of partial agglomeration, or be a consequence of the coating formation itself. In both cases, they were found to be not detrimental for the functionality of the active material. Apart from surface aggregates, which look typical for inkjet printing, surface morphology was found to be similar to micro-plotter printed CuO nanoparticles films.[40] AFM was performed during the different stages of the manufacturing to investigate the morphology and the roughness of the different layers. Figure 3b shows the topographic characterization of the basal SS layer. Lamination signs are clearly visible in the image. Average roughness (R_a) was found to be 14.89 nm on the 20 μm/20 μm scan size. After depositing the strike Ni layer and the Pt coating, R_a increased to 17.08 nm (20 μm/20 μm scan size; Figure 3c). The typical nodular structure of an electrodeposited layer is clearly visible in the image superimposed to the original striped appearance of the SS layer. Figure 3d depicts the AFM analysis of the Pt coating with CuO printed on top. The same aggregates visible in Figure 3a are evident also in Figure 3d. R_a further increases to 38.74 nm, always on the 20 μm/20 μm scan size. The major increase in roughness is for the most part ascribable to the presence of the aggregates, which are hundreds on nanometers high in some cases. Samples were sectioned to visualize the internal structure of the layers and to quantify their thickness. Figure 4a depicts the result obtained with the same sample depicted in Figure 3a. The first strike Ni layer, with a thickness of 650 nm, is clearly visible directly on top of SS. The second Pt layer is visible as well, but the interface with the CuO top coating is not well defined. Thickness of Pt is around 350 nm, while thickness of CuO is between 170 nm and 220 nm. Figures from 4b to 4f show the elemental mapping of the different layers. The pictures demonstrate the distribution of the different layers on the section. From the mechanical stability point of view, CuO NPs layer obtained from inkjet printing were found to be strongly adherent to Pt (after the annealing process). CuO coatings easily resisted simple peel tests performed using Kapton polyimide tape and were found to be water stable.

Sensor performances evaluation.—To use it as a sensor, the SS substrate with the different layers on top was prepared as visible in Figure 5a. The manufacturing procedure described in the experimental methods was followed. Voltammetry was performed on the active material to investigate glucose oxidation on it (Figure 5b). No redox activity was observed on the CuO coated surface in the absence of glucose in the electrolyte. As soon as glucose was added to the NaOH solution, anodic features started to appear. The typical glucose oxidation peak (marked as Glu in Figure 5b) was observed between 0.5 and 0.55 V SCE. The presence of this peak is explained by the glucose oxidation mechanism described by Equations 4 and 5.

$$CuO + OH^- \rightarrow CuOOH + e^- \quad [4]$$

$$CuOOH + e^- + \text{glucose} \rightarrow CuO + OH^- + \text{gluconic acid} \quad [5]$$

Glucose oxidation was reported to be mediated by the formation of Cu(III) as a consequence of the potential increase, according to a mechanism still not well understood.[53] 0.5 V SCE was used as potential to test the electrochemical response of the sensor in potentiostatic tests. Current was recorded as a function of time and increasing amounts of glucose were added to the 0.1 M NaOH solution.

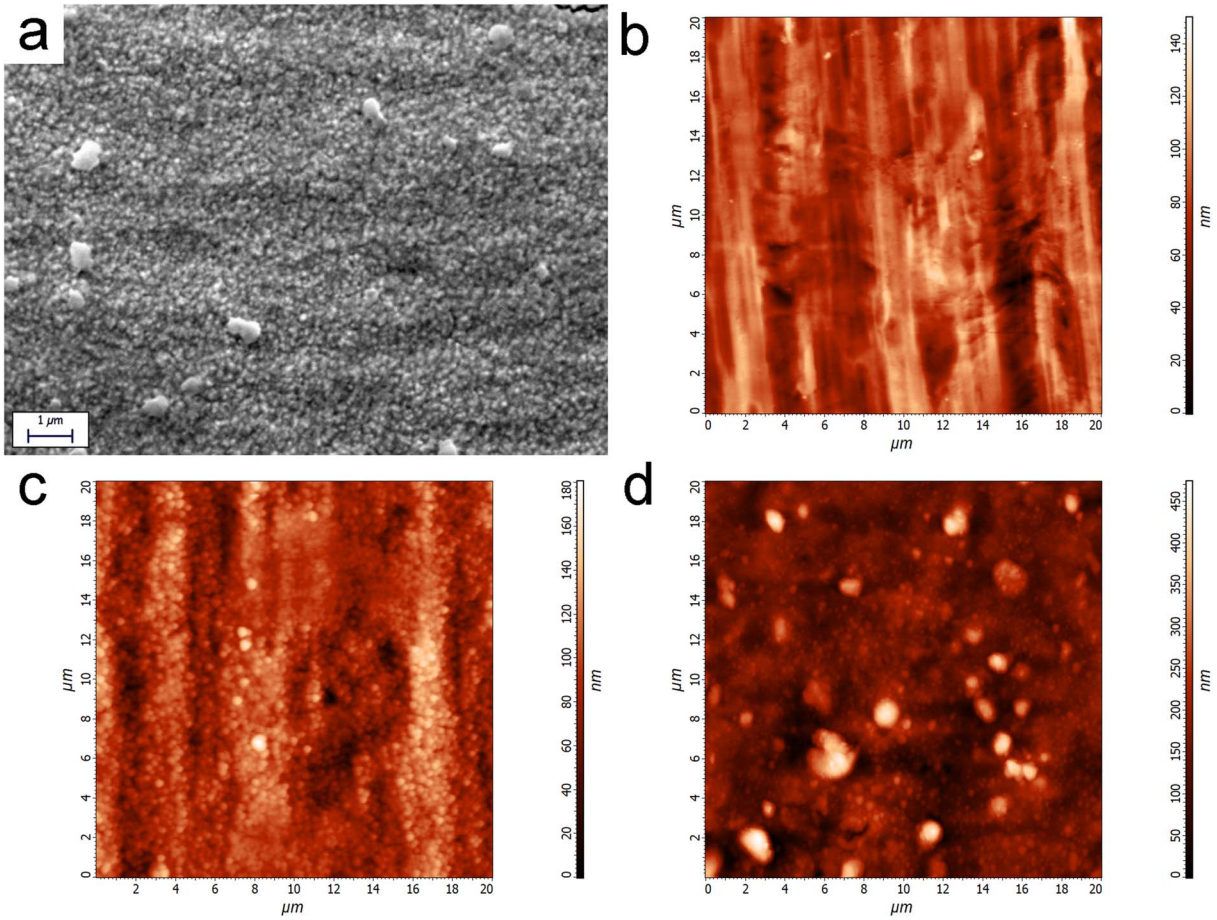

Figure 3. SEM image of the CuO printed surface (a); AFM analysis of SS (b); AFM analysis of the electrodeposited Pt/Ni layers on SS (c); AFM analysis of the CuO printed layer (d).

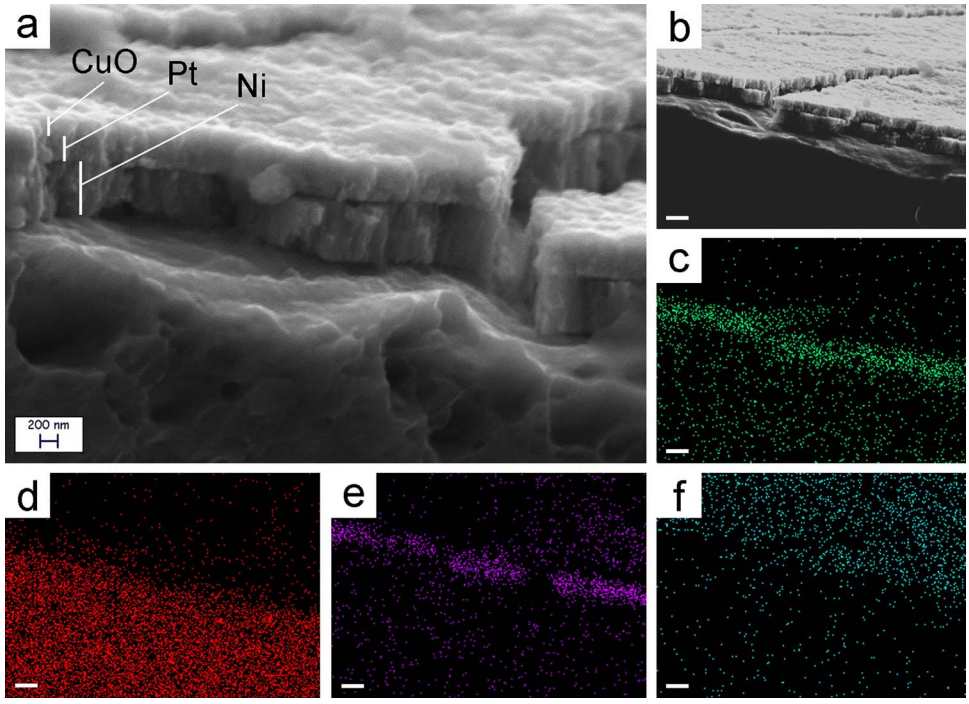

Figure 4. SEM analysis of the CuO/Pt/Ni layers on SS (a); EDS elemental mapping on the section of the CuO/Pt/Ni layers: morphological image (b), Ni (c), Fe (d), Pt (e) and Cu (f). White size bars are 1 μm long.

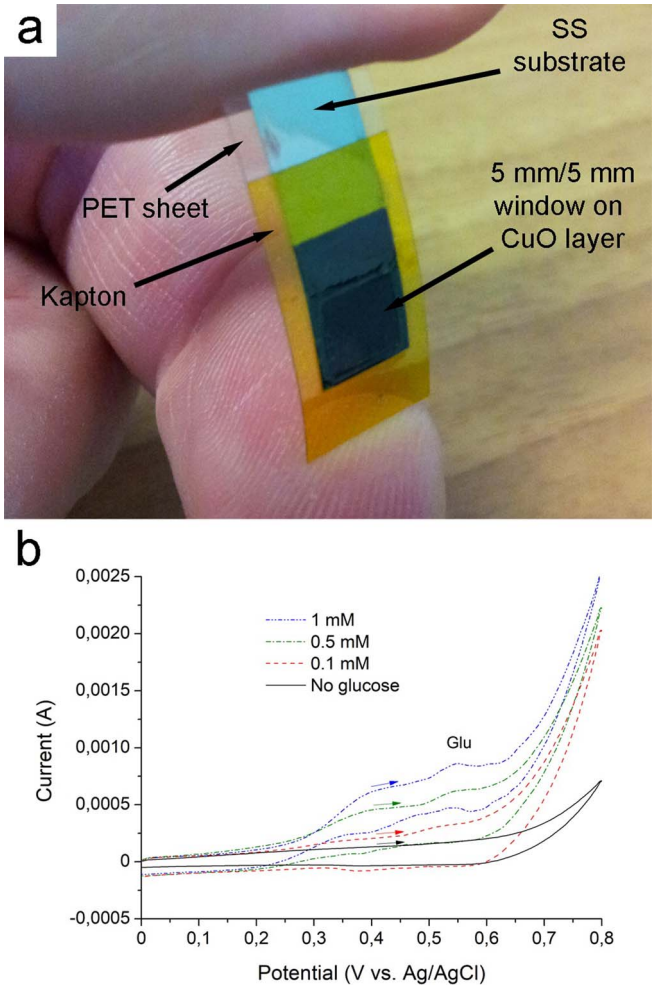

Figure 5. Appearance of the final assembled sensor (a); voltammetry performed in the presence of various glucose amounts (b).

Figure 6a shows the raw curve obtained at the end of the test, where glucose concentration was ranged between 1 and 7 mM with 1 mM steps. The noise visible in the signal recorded was a consequence of the stirring used during the test to favor uniform distribution of glucose in the electrolyte. Noise levels were greater at high glucose concentrations. However, a clear response to the presence of glucose can be seen from Figure 6a. Current values were mediated inside each step and obtained values were used to construct the calibration curve of the inkjet printed CuO sensor (Figure 6b). Due to the low cost approach followed for the manufacturing of the sensor, which was printed using a simple office inkjet printed instead of a laboratory printer, reproducibility may be an issue. For this reason, a second sensor (identical to the first) was built and analyzed. The response of the two sensors was found to be almost identical and reasonably linear up to 6mM. Parameters extrapolated from the linear fitting (limited to the 0–6 mM glucose concentration range) are reported in Table II. Sensitivities differ of only 4.3%, which is an acceptable level for a sensor printed using an office printer. In general, measured sensitivity is in agreement with state of the art sensors analogous to the one presented.[40,43] Linearity was found to decline after 6 mM glucose concentration, as already observed for analogous CuO NPs based sensors.[40,43] However, sensitivity is considerably high in an acceptable linear range. Moreover, such high sensitivity was obtained using a comparatively thin CuO layer with respect to other homologous sensors.[40] After validating sensor functionality, some adjunctive tests were performed to fully characterize the device. In particular, minimum detection limit, sensitivity to interfering species and sensitivity to curvature were investigated. Figure 7a reports the results obtained in the case of the minimum detection limit analysis. Figure 7b shows a magnification of the data visible in Figure 7a. To evaluate the detection limit, glucose concentration was increases by 0.5 μM steps until a signal was clearly detected. Addition of such small glucose concentrations produced a sharp current peak on the working electrode, which immediately decayed due to stirring and homogenization of the electrolyte. After stabilization, current values were mediated in each step and a discernible current step was observed also at 0.5 μM glucose concentration (Figure 7b). This consideration implies that the sensor, similarly to analogous sensors described in the literature, is able to detect very low glucose amounts, down to 0.5 μM. The effect of interfering species on the performances of the sensor was evaluated adding suitable chemical species to the electrolyte in low concentration, as evidenced in Figure 8a. Some interfering species typically present in human blood, like ascorbic acid or uric acid, were

Table II. Performances of two identical inkjet printed CuO glucose sensors.

Sensor	Linear range (mM)	Correlation coefficient	Sensitivity ($\mu A\ mM^{-1}\ cm^{-2}$)
1	1–6	0.9983	1588 ± 25
2	1–6	0.9975	1660 ± 31

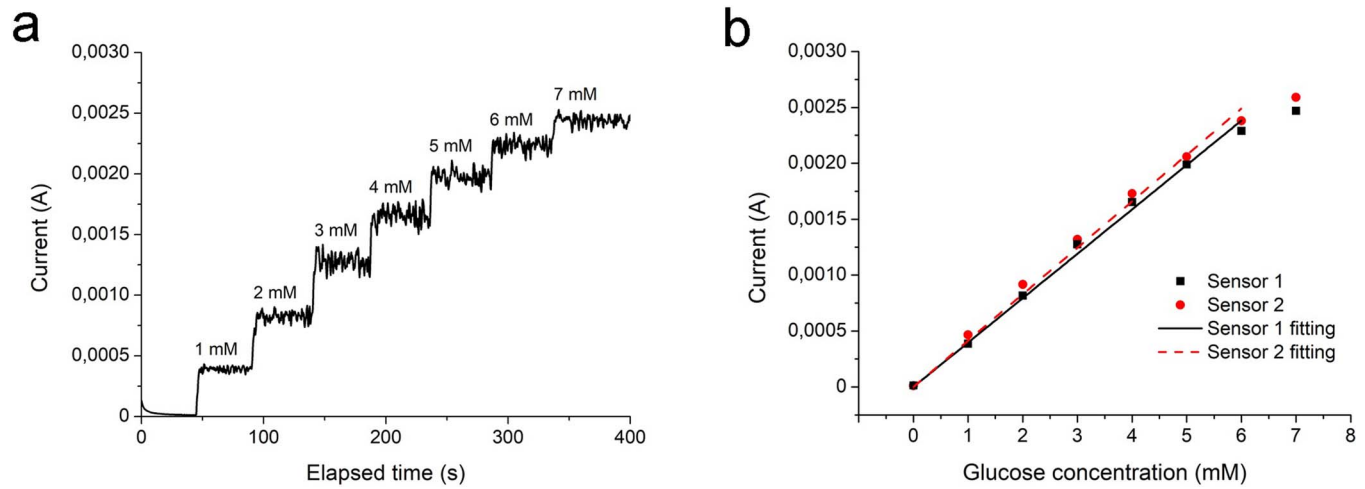

Figure 6. Raw electrochemical response of the sensor (a); calibration curves obtained for two distinct sensors manufactured in the same way (b).

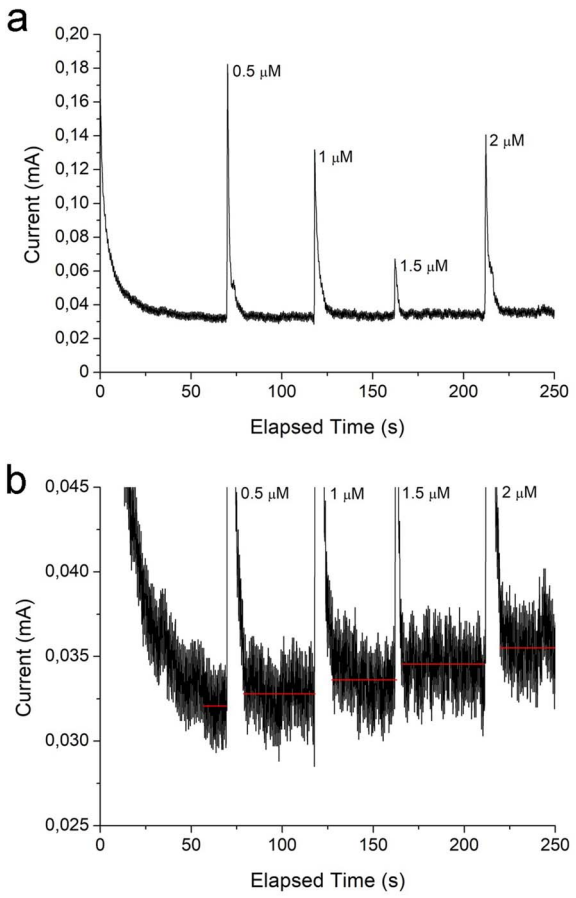

Figure 7. Minimum detection limit test results (a); magnification of the minimum detection limit test results with superimposed mean current values for each step (b).

not considered due to their recognized low interfering power in alkaline electrolytes.[40] On the contrary, many different sugars possibly present in human serum were evaluated as interfering species to investigate sensor selectivity. Two concentration of interfering species, namely 0.01 mM and 0.02 mM, were employed, while 0.5 mM was selected as glucose concentration. Such concentrations are realistic,

Table III. Performances of curved inkjet printed CuO glucose sensors.

Curvature radius	Correlation coefficient	Sensitivity ($\mu A\ mM^{-1}\ cm^{-2}$)
Not flexed	0.9983	1588 ± 25
30 mm	0.9968	1420 ± 31
15 mm	0.9931	1379 ± 43

since concentration of interfering species are typically 30 to 50 times lower than glucose.[54] During the test, an initial glucose amount was added to the electrolyte. Interfering chemicals were then subsequently added, followed by a second glucose amount. As visible in Figure 8a, the presence of many different sugars in the NaOH solution does not provide a significant interference. Finally, the effect of curvature on the performances of the sensor was evaluated (Figure 8b). Two visible effects were recorded from the calibration performed on flexed samples: loss of linearity and loss of sensitivity. Table III reports the parameters obtained from the linearization (limited to the 0–6 mM glucose range) of the data presented in Figure 8b. Loss of linearity is evident from the progressive decrease of the correlation coefficient extrapolated from data linearization. Conversely, sensitivity decreased as well. A possible explanation for the deterioration of the performances is the progressive damaging of the CuO layer according to a cracking mechanism. When the device is flexed, cracks may form on the surface, allowing contact of the electrolyte with the Pt layer and decreasing charge transfer. Sensitivity reduction as a consequence of bending has already been observed in CuO thin films based glucose sensors.[55]

Integration in USNs.—The single use flexible sensor described in the present manuscript must be coupled with a reusable device containing electronic circuits required for signal readout and power supply. Such device can be connected via low energy Bluetooth to a smartphone or directly to a router to allow data transfer, following an approach described in the existing literature.[56] By doing this, information about glucose levels for a specific patient can be easily send in real time and in a continuous way to health facilities to allow efficient diabetes monitoring.

Conclusions

The development of a single-use flexible electrochemical glucose sensor employing CuO nanoparticles as active material was carried out. Such device was obtained coupling a conductive sheet, plated with Ni/Pt and inkjet printed with CuO NPs, with a PET supporting layer. Low cost techniques, including inkjet printing from office

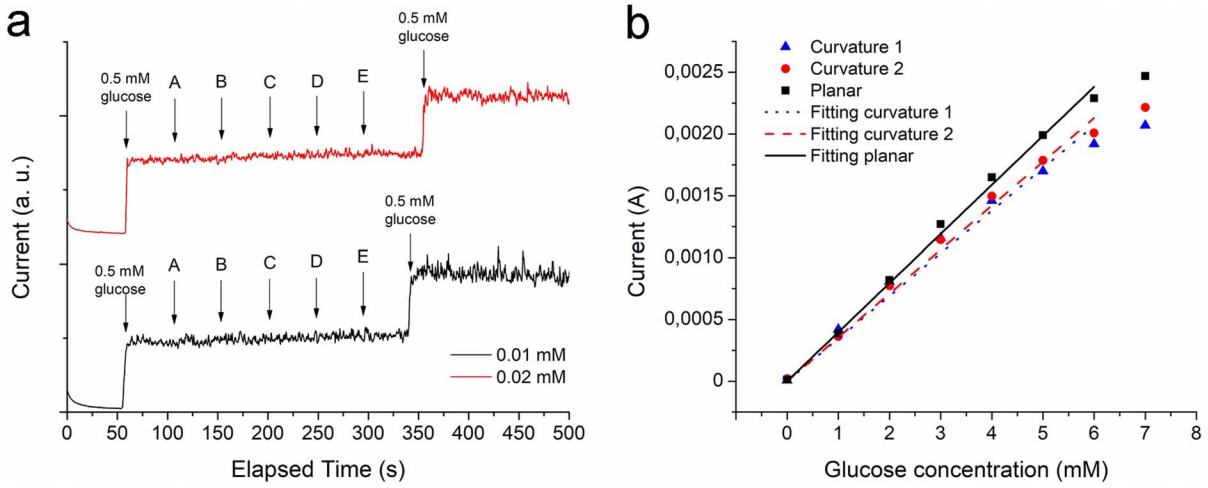

Figure 8. Interference performances test results for two values of interfering species concentration (a): A = lactose, B = mannitol, C = maltose, D = sorbitol, E = fructose; calibration curves obtained for curved sensors compared with data from planar samples from Figure 6b (b).

printers and wet metallization, were employed to accomplish the task. Sensor manufacturing showed in general a good reproducibility and the devices obtained were characterized by a high sensitivity (around 1600 μA mM^{-1} cm^{-2}) and a wide linear range. A low detection limit, coupled with a good insensitivity toward other sugars that may be present in blood, was demonstrated as well. Finally, the behavior of the sensor in curved configuration was studied, evidencing a loss in sensitivity and linearity as a consequence of possible damaging in the active CuO layer. The sensors described in the present work, characterized by an ultra-low cost manufacturing route, may be interesting candidates for applications requiring high customizability, wearability, low cost per unit and scalability. All these requirements are the ones typical of proposed USNs for diabetes monitoring.

Acknowledgments

The work described in the text was carried out in the framework of the interdepartmental laboratory MEMS&3D at Politecnico di Milano, Milano, Italy.

ORCID

L. Magagnin https://orcid.org/0000-0001-5553-6441

References

1. W. Lutz, W. Sanderson, and S. Scherbov, *Nature*, **451**, 716 (2008).
2. J.-Y. Tsauo, W.-S. Leu, Y.-T. Chen, and R.-S. Yang, *Arch. Phys. Med. Rehabil.*, **86**, 1953 (2005).
3. Á. Jobbágy et al., in *14th Nordic-Baltic Conference on Biomedical Engineering and Medical Physics*, p. 454, Springer (2008).
4. S. Patel, H. Park, P. Bonato, L. Chan, and M. Rodgers, *J. Neuroeng. Rehabil.*, **9**, 21 (2012).
5. K. Hung, Y.-T. Zhang, and B. Tai, in *Engineering in Medicine and Biology Society, 2004. IEMBS'04. 26th Annual International Conference of the IEEE*, vol. **2**, p. 5384, IEEE (2004).
6. Y.-L. Zheng, B. P. Yan, Y.-T. Zhang, and C. C. Y. Poon, *IEEE Trans. Biomed. Eng.*, **61**, 2179 (2014).
7. J. J. Mastrototaro, *Diabetes Technol. Ther.*, **2**, 13 (2000).
8. D. Bandyopadhyay and J. Sen, *Wirel. Pers. Commun.*, **58**, 49 (2011).
9. Z. Tafa, in *Application and Multidisciplinary Aspects of Wireless Sensor Networks*, p. 267, Springer (2011).
10. C.-Y. Chong and S. P. Kumar, *Proc. IEEE*, **91**, 1247 (2003).
11. I. A. Essa, *IEEE Pers. Commun.*, **7**, 47 (2000).
12. G.-Z. Yang and G. Yang, *Body sensor networks*, Springer, (2006).
13. R. Istepanian, S. Laxminarayan, and C. S. Pattichis, *M-health*, Springer, (2006).
14. A. Darwish and A. E. Hassanien, *Sensors*, **11**, 5561 (2011).
15. E. Jovanov and A. Milenkovic, *J. Med. Syst.*, **35**, 1245 (2011).
16. J. Ko et al., *Proc. IEEE*, **98**, 1947 (2010).
17. Y.-D. Lee and W.-Y. Chung, *Sensors Actuators B Chem.*, **140**, 390 (2009).
18. S. A. Munir et al., in *Advanced Information Networking and Applications Workshops, 2007, AINAW'07. 21st International Conference on*, vol. **2**, p. 113, IEEE (2007).
19. M. Patel and J. Wang, *IEEE Wirel. Commun.*, **17** (2010).
20. A. Pantelopoulos and N. G. Bourbakis, *IEEE Trans. Syst. Man, Cybern. Part C (Applications Rev.*, **40**, 1 (2010).
21. C. Bachmann et al., *IEEE Commun. Mag.*, **50** (2012).
22. R. Mukkamala et al., *IEEE Trans. Biomed. Eng.*, **62**, 1879 (2015).
23. S. Kumar, K. Kambhatla, F. Hu, M. Lifson, and Y. Xiao, *Int. J. Telemed. Appl.*, **2008**, 3 (2008).
24. N. D. D. Group, *Diabetes*, **28**, 1039 (1979).
25. http://www.diabetesatlas.org.
26. O. Karan, C. Bayraktar, H. Gümüşkaya, and B. Karlık, *Expert Syst. Appl.*, **39**, 54 (2012).
27. M. Ezzati et al., *Lancet Diabetes Endocrinol.*, **5**, 162 (2017).
28. J.-H. Cho et al., *Korean Diabetes J.*, **34**, 267 (2010).
29. R. S. H. Istepanian, S. Hu, N. Y. Philip, and A. Sungoor, in *Engineering in Medicine and Biology Society, EMBC, 2011 Annual International Conference of the IEEE*, p. 5264, IEEE (2011).
30. A. J. Jara, M. A. Zamora, and A. F. G. Skarmeta, *Pers. Ubiquitous Comput.*, **15**, 431 (2011).
31. G. Wang et al., *Microchim. Acta*, **180**, 161 (2013).
32. S. Park, H. Boo, and T. D. Chung, *Anal. Chim. Acta*, **556**, 46 (2006).
33. N. S. Oliver, C. Toumazou, A. E. G. Cass, and D. G. Johnston, *Diabet. Med.*, **26**, 197 (2009).
34. K. Tian, M. Prestgard, and A. Tiwari, *Mater. Sci. Eng. C*, **41**, 100 (2014).
35. A. J. Bandodkar and J. Wang, *Trends Biotechnol.*, **32**, 363 (2014).
36. X. Niu et al., *RSC Adv.*, **6**, 84893 (2016).
37. M. M. Rahman, A. J. Ahammad, J.-H. Jin, S. J. Ahn, and J.-J. Lee, *Sensors*, **10**, 4855 (2010).
38. Y. Song, K. Qu, C. Zhao, J. Ren, and X. Qu, *Adv. Mater.*, **22**, 2206 (2010).
39. D. Jiang et al., *Biosens. Bioelectron.*, **54**, 273 (2014).
40. A. Molazemhosseini, L. Magagnin, P. Vena, and C.-C. Liu, *J. Electroanal. Chem.*, **789**, 50 (2017).
41. N. Lu et al., *Ceram. Int.*, **42**, 11285 (2016).
42. Y. Zhong et al., *Sensors Actuators B Chem.*, **236**, 326 (2016).
43. R. Ahmad, M. Vaseem, N. Tripathy, and Y.-B. Hahn, *Anal. Chem.*, **85**, 10448 (2013).
44. E. Reitz, W. Jia, M. Gentile, Y. Wang, and Y. Lei, *Electroanalysis*, **20**, 2482 (2008).
45. S. Gopinath and J. Philip, *Mater. Chem. Phys.*, **145**, 213 (2014).
46. A. Kamyshny and S. Magdassi, in *Inkjet-Based Micromanufacturing*, p. 173, Wiley-Blackwell (2012).
47. S. Sonia et al., *Mater. Sci. Semicond. Process.*, **30**, 585 (2015).
48. D. Jang, D. Kim, and J. Moon, *Langmuir*, **25**, 2629 (2009).
49. S. G. Mallinson, G. D. McBain, and G. D. Horrocks, in *20th Australasian Fluid Mechanics Conference Perth, Australia 5–8 December 2016*, (2016).
50. R. L. Fogel'son and E. R. Likhachev, *Tech. Phys.*, **46**, 1056 (2001).
51. S. Mueller, E. W. Llewellin, and H. M. Mader, in *Proceedings of the Royal Society of London A: Mathematical, Physical and Engineering Sciences*, p. rspa20090445, The Royal Society (2009).
52. J. E. Fromm, *IBM J. Res. Dev.*, **28**, 322 (1984).
53. N. Torto, T. Ruzgas, and L. Gorton, *J. Electroanal. Chem.*, **464**, 252 (1999).
54. C. Zhou et al., *Sci. Rep.*, **4**, 7382 (2014).
55. J. Huang et al., *Nanoscale*, **7**, 559 (2015).
56. B. Massot, N. Noury, C. Gehin, and E. McAdams, in *e-Health Networking, Applications & Services (Healthcom), 2013 IEEE 15th International Conference on*, p. 310, IEEE (2013).